# Atomic Scale Conductance Induced by Single Impurity Charging

N. A. Pradhan, N. Liu, C. Silien,* and W. Ho†

*Department of Physics and Astronomy and Department of Chemistry, University of California, Irvine, California 92697-4575, USA*

(Received 3 September 2004; published 23 February 2005)

A scanning tunneling microscope was used to probe electron transport through an alkali doped $C_{60}$ monolayer crystal on $Al_2O_3$ grown by the oxidation of NiAl(110). Each individual alkali atom forms a localized complex with the neighboring $C_{60}$ molecules. Charging of the complex induces a substantial rise in the current that persists outside the physical dimensions of the complex. This induction of the current rise is characterized by spatially resolved spectroscopy and mapping of the differential conductance ($dI/dV$) in the vicinity of the complex.

DOI: 10.1103/PhysRevLett.94.076801 PACS numbers: 73.61.Wp, 73.63.–b, 85.35.–p, 85.65.+h

The reduction of electronic devices to the nanometer scale is a scientific and technological quest, aided by advances in experimental techniques and theoretical understanding [1,2]. It has now become possible to observe both charge and energy quantization since the advent of nanofabricated break junctions [3,4] and single molecule transistors [5,6]. The transistor geometry is naturally suited for probing the effects of impurities on the transport [7]. However, knowledge of the location and structure of the impurities has remained elusive. While the scanning tunneling microscope (STM) is known to image and resolve orbitals of single molecules [8,9] and charge states of single atoms [10], the technique relies on measuring the conductance between two electrodes. In this Letter, we demonstrate the ability of the STM to spatially image and characterize the single impurities and to control the atomic scale conductance by the nonlocal charging of a single impurity in a double barrier tunneling junction (DBTJ).

The homemade variable temperature ultrahigh vacuum STM used to perform the experiments is based on a design detailed in the literature [11]. In order to observe the reported phenomenon, we first grew a thin $Al_2O_3$ film on NiAl(110) in a manner described elsewhere [12]. $C_{60}$ (Aldrich, 99.9% purity) was then sublimated from an alumina crucible onto the oxidized surface at room temperature. The alkali atoms (SAES Getters) were deposited onto the $C_{60}/Al_2O_3/NiAl(110)$ surface after cooling to 11 K. The tips were etched from polycrystalline Ag wire with a diameter of 0.020″. The differential conductance ($dI/dV$) was measured with lock-in detection of the ac tunneling current by modulating the sample bias ($\sim 10$ mV, $\sim$260 Hz) while keeping the feedback loop open. All measurements were carried out at 11 K, at a base pressure lower than $3 \times 10^{-11}$ Torr.

The DBTJ consists of a Ag tip, a vacuum barrier, an alkali doped $C_{60}$ monolayer, an $Al_2O_3$ insulating layer, and a NiAl(110) substrate [Fig. 1(a)]. By choosing this geometry, we can separate the alkali doped $C_{60}$ monolayer from either electrode. From the STM topographic images [see Figs. 2 and 3(a)], the $C_{60}$ monolayer has a triangular structure with a lattice constant of about 10 Å, albeit with varying molecular orientations. The $dI/dV$ spectra exhibit a conductance gap from $-2.4$ to $+0.45$ V (Fig. 2). Since the spectra show little variation with the tip positioned over different locations in the $C_{60}$ layer, we infer that adsorption over the $Al_2O_3$ film ($\sim$5 Å thick) leads to the formation of a two-dimensional $C_{60}$ band structure [8]. The $C_{60}$ monolayer was systematically doped with Na, K, Rb, and Cs to reveal the relationship between the dopant-host bonding and conductance gating. All the alkali metals react predominantly with the nearest neighbor $C_{60}$ and form well-defined impurity complexes in the $C_{60}$ monolayer. We shall mainly use the results from Cs to discuss the general phenomenon.

The Cs atoms appear as protrusions centered on the threefold hollow sites of the $C_{60}$ lattice. The $dI/dV$ spectra associated with the $Cs(C_{60})_3$ complex display intense, sharp conductance peaks, $\boldsymbol{H}$ and $\boldsymbol{L}$, at both polarities of bias (see the bottom of Fig. 2). In Fig. 1(b), we present an energy level diagram directly over the $Cs(C_{60})_3$ complex for the sharp peak $\boldsymbol{H}$ at positive bias. The origin of this peak is tied to the first peak $\boldsymbol{h}$ of a progression of vibronic states at the negative bias (Fig. 2). This progression is within the highest occupied molecular orbital (HOMO) of the complex, [12,13] located at energy $\Delta$ below the Fermi level ($E_F$) at zero bias. As the sample bias $V_b$ is increased ($V_b > 0$), the voltage at the $Cs(C_{60})_3$ complex $V_a$ also increases in proportion to the voltage division across the DBTJ. When $V_a$ reaches $\Delta$, the HOMO state aligns with the $E_F$ (NiAl), leading to the ionization (positive charging) of the impurity.

Figures 1(b) and 1(c) show the energy diagrams just before and after the threshold of ionization, respectively. The $C_{60}$ band $\boldsymbol{B}$ is shown partially below $E_F$ (tip) at bias $V_{b1}$ in accordance with the $dI/dV$ spectra. At the ionization threshold, the positive ion creates an attractive potential that pulls down the $C_{60}$ band to $\boldsymbol{B}'$ [see Fig. 1(c)], thus increasing the density of states for electron transport, in addition to the opening of the conductance channel involv-

 © 2005 The American Physical Society

ing the HOMO. This results in a sizeable step in the tunneling current and a corresponding sharp peak in $dI/dV$ at $V_{b2}$. This mechanism is possible due to the finite voltage drop across the oxide film in addition to that across the vacuum barrier. The much higher impedance across the vacuum junction than that across the oxide precludes any conductance peaks due to charge accumulation within the complex [14]. This interpretation, based on the relative tunneling rates between the two barriers, is corroborated by similar observations on isolated Cu(II)-phthalocyanine molecules adsorbed on an $Al_2O_3$/NiAl(110) surface [15].

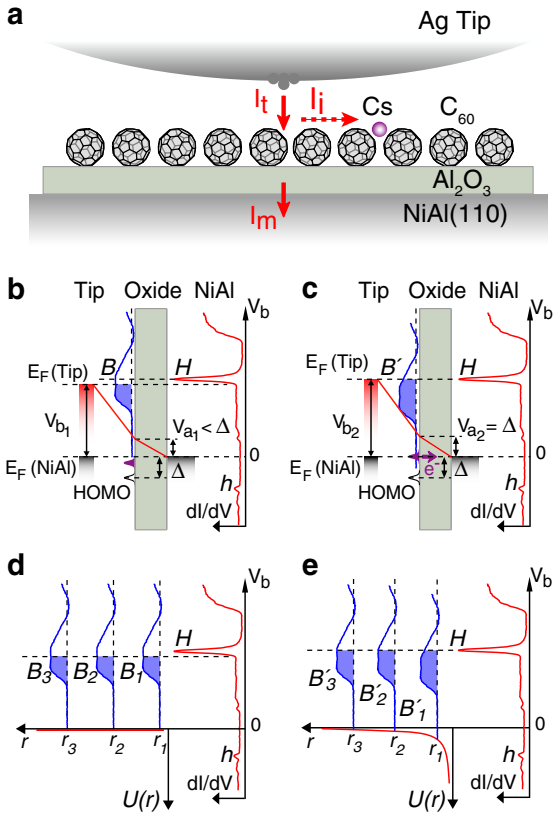


FIG. 1 (color online). Mechanism and effect of impurity ionization on electron transport. (a) Schematic diagram of the tunneling geometry, showing the relative position of the silver tip, Cs impurity on $C_{60}$ monolayer, $Al_2O_3$ film, and the NiAl(110) substrate. The directions of electron transport (for positive bias, $V_b > 0$) are indicated by the arrows. $I_t$, $I_m$, and $I_i$ are discussed in the text. (b),(c) Energy diagram of the tunneling process with the tip positioned over the Cs impurity just before (b) and crossing (c) the threshold of ionization. Upon ionization, a new conducting channel is opened, involving the HOMO, and the $C_{60}$ band $\boldsymbol{B}$ is down-shifted to $\boldsymbol{B}'$, leading to an increase in the number of states available for transport. This results in the sharp peak $\boldsymbol{H}$ which is correlated with the peak $\boldsymbol{h}$ associated with the HOMO state observed at negative bias. (d),(e) The energy of the $C_{60}$ bands at three different radial distances from the complex, just before (d) and crossing (e) the threshold of ionization. Impurity ionization gives rise to the lateral potential $U(r)$ that shifts the bands downwards.

In Figs. 1(d) and 1(e), the $C_{60}$ bands $\boldsymbol{B}_1$, $\boldsymbol{B}_2$, and $\boldsymbol{B}_3$ are shown for three lateral distances $r$ between the tip and the complex. The ionization of the $Cs(C_{60})_3$ complex creates an attractive potential $U(r)$ that is expected to extend a few $C_{60}$ lattice constants within the monolayer. In comparison to $V_{a1} < \Delta$, $\boldsymbol{B}_1$, $\boldsymbol{B}_2$, and $\boldsymbol{B}_3$ are lowered in energy to $\boldsymbol{B}'_1$, $\boldsymbol{B}'_2$, and $\boldsymbol{B}'_3$, respectively, according to the value of $U(r)$ at their respective locations [Fig. 1(e)]. The shift of band $\boldsymbol{B}$ to

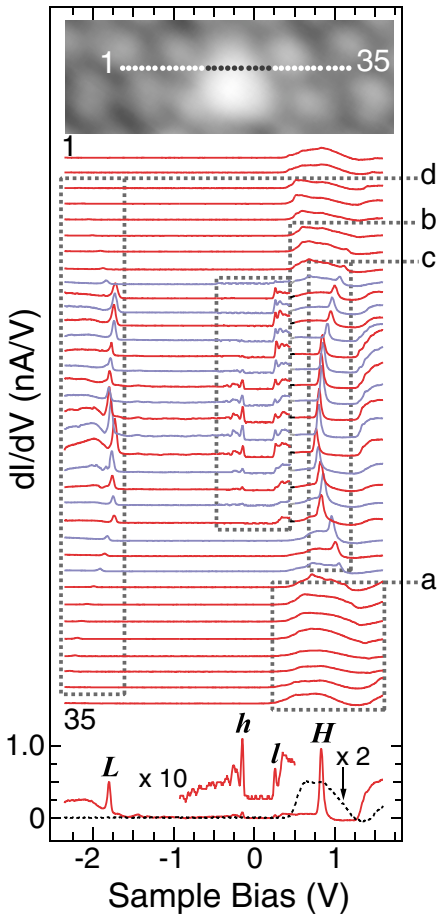


FIG. 2 (color online). Spatial mapping of the differential conductance measured at 35 points across a $Cs(C_{60})_3$ complex; spectra are offset for clarity. A $dI/dV$ spectrum measured directly over the impurity is shown at the bottom, along with the spectrum measured over the $C_{60}$ monolayer away from the complex (dotted line). The peaks associated with the HOMO ($\boldsymbol{h}$, $\boldsymbol{H}$) and LUMO ($\boldsymbol{l}$, $\boldsymbol{L}$) are indicated. The distinct features in the spectra are highlighted in four zones, corralled by the dotted lines. Zone $a$ shows the $C_{60}$ band away from the $Cs(C_{60})_3$ complex. Zone $b$ shows the electronic structure close to $E_F$ of the sample. The conductance gap about $E_F$ is reduced over the complex due to charge transfer between the Cs adatom and the underlying $C_{60}$ molecules. The spectra in this zone have been magnified by a factor of 4.5 to highlight the weak features near $E_F$. The occurrence and energy shift of peak $\boldsymbol{H}$ is seen in zone $c$. Zone $d$ displays peak $\boldsymbol{L}$ associated with the negative charging of the LUMO peak $\boldsymbol{l}$.

$B'$, and the corresponding increase in the density of states available for transport, decreases as $r$ increases. Since the magnitude of the conductance peak is proportional to the density of states made available due to the band shift, the peak height will tend to decrease for points away from the complex. In addition, a larger ionization threshold is required when the tip is moved parallel to the surface away from the complex due to the positive tip curvature causing an increase in the tip-complex distance. Thus the value of $U(r)$, the $C_{60}$ density of states, and the emergence of conduction involving the HOMO of the alkali-$C_{60}$ complex determine the magnitude of the switching action associated with the impurity ionization.

A spatial mapping of the $dI/dV$ spectra at 35 positions across a $Cs(C_{60})_3$ complex, as marked in the topographic image, is displayed in Fig. 2. Away from the complex, the $C_{60}$ band structure is unperturbed, indicating the finite range of the impurity potential (zone *a*). Rich structures are observed on both sides of the conductance gap, reduced to 0.4 V, and localized on the $Cs(C_{60})_3$ complex (zone *b*). From the discussion above, as the tip is moved away from the impurity, the magnitude of the sharp peak ***H*** decreases and its position is shifted to higher bias $V_b$. The sharp peak ***L***, associated with the filling of the lowest unoccupied molecular orbital (LUMO) ***l*** (negative charging), exhibits qualitatively a similar behavior (zone *d*) [16].

The onset of the ionization can be visualized by imaging the spatial distribution of the $dI/dV$ signal [Fig. 3(a)] for different values of the sample bias (Fig. 3). The $dI/dV$ images were recorded along with the topographic image with the tunneling gap set with 0.1 nA and 1.65 V. For bias values lying in the $C_{60}$ band gap, we see that the $dI/dV$ intensity is localized over the complex [Fig. 3(a), 2–4]. Above 0.45 V, the surrounding $C_{60}$ monolayer also contributes to the conductance [Fig. 3(a), 5–8]. At the ionization threshold, a strong $dI/dV$ signal is observed to be localized on the $Cs(C_{60})_3$ complex [Fig. 3(a), 7]. Above the threshold, the localized image evolves into a ring centered on the complex [Fig. 3(a), 8]. This ring is the locus of all the tip positions where the ionization occurs for a given bias or equivalently where peak ***H*** in Fig. 2 is located. From zone *c* of Fig. 2, we see that the lowest bias value for peak ***H*** occurs directly over the impurity. For a higher bias value, there are two points, one on each side of the impurity, where peak ***H*** is observed. For different mapping directions, these pairs of points define a ring in the corresponding $dI/dV$ image.

The results for the alkali impurities on $C_{60}/Al_2O_3/NiAl(110)$ are not observed for alkali atoms adsorbed either on the $Al_2O_3$ film or on the $C_{60}$ monolayer on the bare NiAl(110) surface. The isolation of the $C_{60}$ monolayer from the NiAl and the Ag tip gives rise to its two-dimensional band character. In Fig. 3(b), the step in the current gives rise to a sharp conductance peak that is associated with the nonlocal ionization of a single impurity. This effect can be further understood by considering the directions of the electron transport in Fig. 1(a). Upon ionization of the impurity, the current originating from the tip, $I_t$, can flow directly through the monolayer and into the metal ($I_m$), or through the impurity ($I_i$), mediated by the $C_{60}$ band. The effect of single impurity charging on the tunneling current is observed in the steplike increase in $I_m$ and the emergence of the $I_i$ channel.

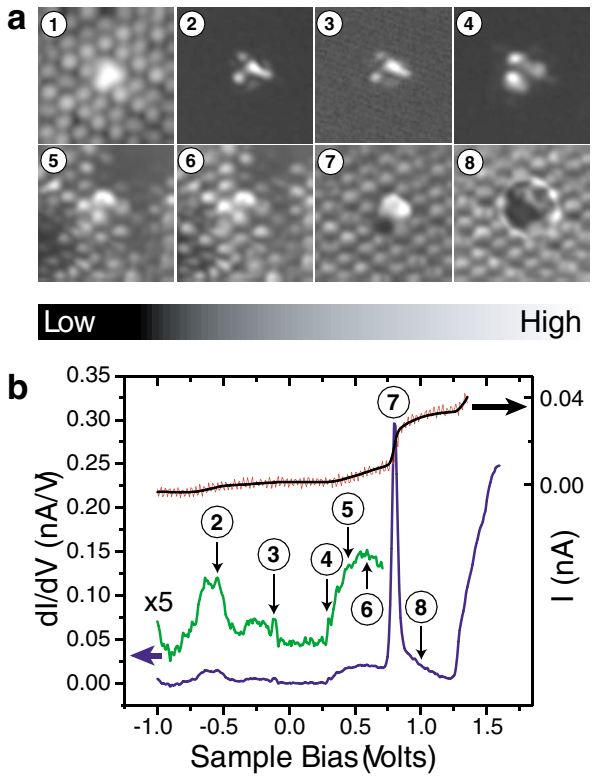


FIG. 3 (color online). Emergence of the ring in the $dI/dV$ images. Image 1 shows the 70 Å × 70 Å topographic image of the $Cs(C_{60})_3$ complex measured at fixed tunneling parameters 0.1 nA and 1.65 V. Images 2–8 show the corresponding $dI/dV$ images at −0.54, −0.1, 0.37, 0.45, 0.56, 0.8, and 1.0 V, respectively. These voltages are marked on the $dI/dV$ spectrum shown below, which is obtained with a tunneling gap fixed at 0.1 nA and 1.65 V. A portion of the $dI/dV$ curve is magnified to reveal the details. The measured $I$-$V$ (jagged line) and the integrated $dI/dV$ (smooth line) curves reveal the step in the current corresponding to the location of the sharp peak in the $dI/dV$ spectrum.

The evolution of the ring with bias across the DBTJ is shown in Fig. 4 for $C_{60}$ doped with Cs, Rb, K, and Na. In the case of Cs, we see that the ring diameter increases with the bias. This is expected from the shift of peak ***H*** in the $dI/dV$ mapping shown in Fig. 2. While a similar behavior is observed for Rb, an opposite trend is found for K and Na, demonstrating the effects of variation in the alkali-$C_{60}$ bonding. It is well known that the alkali-$C_{60}$ bonding is sensitive to molecular orientation as well as to the size of

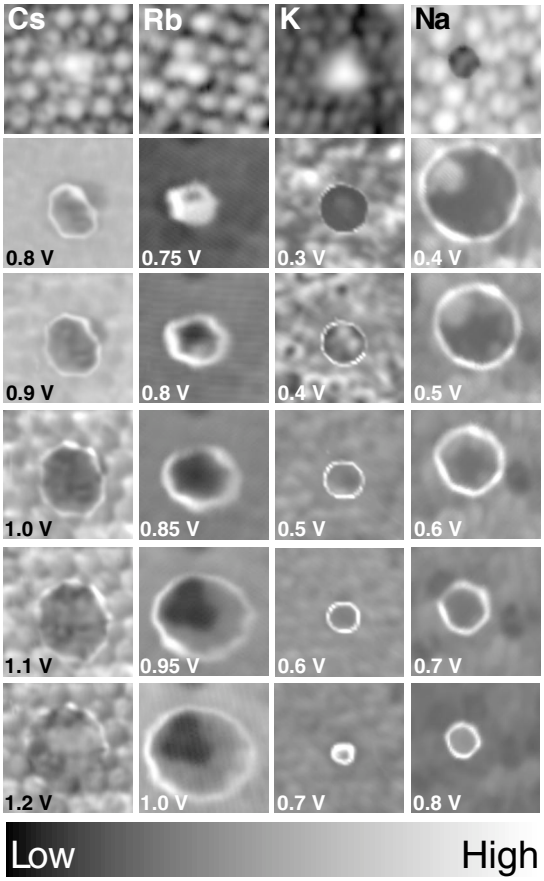


FIG. 4. $dI/dV$ microscopy images on $C_{60}/Al_2O_3/NiAl(110)$ of isolated Cs (50 Å × 50 Å, gap set at 0.1 nA and 1.0 V), Rb (47 Å × 47 Å, gap set at 0.1 nA and 1.25 V), K (65 Å × 65 Å, gap set at 35 pA and 1.0 V), and Na (40 Å × 40 Å, gap set at 0.1 nA and 1.0 V) complexes as a function of the bias voltage. The first image in each column shows the corresponding topographic image of each complex.

the alkali atoms [17]. Because of their smaller size, it is possible that K and Na bond differently to the underlying $C_{60}$ layer as compared to Rb and Cs [18]. However, the precise mechanism of this variation in electronic properties is presently unknown. An understanding into the nature of the alkali-$C_{60}$ bonding in our DBTJ geometry would challenge *ab initio* calculations.

This Letter demonstrates the phenomenon that an electric field resulting from the charging of a single impurity can trigger a stepwise increase in current that is spatially confined to atomic dimensions and removed from the impurity. The ability to control the current in a DBTJ by changing the position of the STM tip with respect to an impurity demonstrates the nonlocal effect on charge transport by the potential gradient from a singly charged impurity. The high spatial resolution provided by the STM also reveals the effects on nanoscale transport due to the nature of the local chemical bonding associated with different alkali impurities. Such understanding suggests a new approach for unraveling the collective effects of impurity doping, e.g., superconductivity in alkali-$C_{60}$ compounds, and the operation of electronic devices at the nanoscale.

This work was supported by the Air Force Office of Scientific Research. The authors are grateful to X. Chen, G. V. Nazin, X. H. Qiu, and S. Wu for many insights and inspiring discussions. C. S. acknowledges support by the Belgian National Fund for Scientific Research (FNRS).

*On leave of absence from Laboratoire de Spectroscopie Moléculaire de Surface, Facultés Universitaires Notre-Dame de la Paix, rue Bruxelles 61, B-5000, Namur, Belgium.
†To whom correspondence should be addressed.
Electronic address: wilsonho@uci.edu

[1] C. Joachim, J. K. Gimzewski, and A. Aviram, Nature (London) **408**, 541 (2000).
[2] A. Nitzan and M. A. Ratner, Science **300**, 1384 (2003).
[3] C. Zhou *et al.*, Appl. Phys. Lett. **71**, 611 (1997).
[4] C. Kergueris *et al.*, Phys. Rev. B **59**, 12 505 (1999).
[5] H. Park *et al.*, Nature (London) **407**, 57 (2000).
[6] W. Liang *et al.*, Nature (London) **417**, 725 (2002).
[7] M. Xiao, I. Martin, E. Yablanovitch, and H. W. Jiang, Nature (London) **430**, 435 (2004).
[8] T. Hashizume *et al.*, Phys. Rev. Lett. **71**, 2959 (1993).
[9] B. C. Stipe *et al.*, Phys. Rev. Lett. **78**, 4410 (1997).
[10] J. Repp, G. Meyer, F. E. Olsson, and M. Persson, Science **305**, 493 (2004).
[11] B. C. Stipe, M. A. Rezaei, and W. Ho, Rev. Sci. Instrum. **70**, 137 (1999).
[12] N. Liu, N. A. Pradhan, and W. Ho, J. Chem. Phys. **120**, 11 371 (2004).
[13] X. H. Qiu, G. V. Nazin, and W. Ho, Phys. Rev. Lett. **92**, 206102 (2004).
[14] I. B. Altfeder and D. M. Chen, Phys. Rev. Lett. **84**, 1284 (2000).
[15] S. W. Wu, G. V. Nazin, X. Chen, X. H. Qiu, and W. Ho, Phys. Rev. Lett. **93**, 236802 (2004).
[16] Peak ***H*** lies in a bias range where it overlaps with the $C_{60}$ band. Peak ***L***, however, does not overlap with the $C_{60}$ band. Thus peak ***L*** arises from the emergence of a new conductance channel when the ***l*** state (LUMO) of the alkali-$C_{60}$ complex is filled. The intensity of the peak ***H*** is higher than that of the peak ***L*** since an additional increase in the conductance arises from the lowering of the $C_{60}$ band as indicated in Fig. 1. The larger shift in ***H*** compared to ***L*** is attributed to the presence of the $C_{60}$ band and the associated bias dependent (including positive and negative biases) voltage division across the junction.
[17] M. S. Dresselhaus, G. Dresselhaus, and P. C. Eklund, *Science of Fullerenes and Carbon Nanotubes* (Academic Press, San Diego, 1996).
[18] This is apparent for Na from the topographic image in Fig. 4, but not for K. Also, the inability to determine the orientations of the $C_{60}$ forming the complex poses another constraint in elucidating the different trends.